Experimental and numerical study on homogenisation of BCV bentonite using dual density samples

Jan Najser[1*] and *David* Mašín[1]

[1]Institute of Hydrogeology, Engineering Geology and Applied Geophysics, Faculty of Science, Charles University, Prague, Czech Republic

Abstract. Homogenisation of bentonite materials is an essential feature for its sealing function in radioactive waste repositories. Presented study is focused on the laboratory investigation of the homogenisation of Czech BCV bentonite (Ca/Mg type). The experimental program included measurement of the swelling pressures of single-density and dual-density samples of the compacted bentonite, where dual-density sample is composed of two layers compacted to two different dry densities. Tests were performed in constant volume cells, which allowed measurement of swelling pressure evolution. Dual-density tests included two identical samples saturated from different sides. Homogenisation was investigated through the determination of the final density distribution in a vertical profile from the post-mortem analysis. Further, the laboratory experiments were simulated by means of a thermo-hydro-mechanical hypoplastic model for bentonite implemented in the SIFEL coupled finite element code. It was found that swelling pressures developed by dual-density samples corresponded well to swelling pressures developed by single density samples of equivalent dry densities, while its time-evolution was different. Dual density samples also revealed very good level of density homogenisation after the test. The first observation (swelling pressure along with its temporal evolution) was predicted well by the model, which however underestimated the level of dry density homogenisation.

1 Introduction

Bentonites are considered as suitable sealing buffer materials for radioactive waste repositories because of their low permeabilities and high swelling potential. However, the placement of the bentonite barrier results in initial heterogeneities which could potentially form preferential pathways for the migration of radionuclides and diminish the sealing function of the buffer.

High-density bentonite pellets have been widely considered to minimise the occurrence of large technological voids and even to substitute the compacted blocks in the bentonite buffer [1-3]. However, pelletised bentonite in its initial state is characterised by extreme density gradients. Therefore, homogenisation of bentonite materials during the saturation is the key feature of the barrier in terms of the effectiveness of its sealing function.

Until recent years, most of the studies on homogenisation investigated transformation of bentonite pellets towards more uniform density distribution upon saturation [4, 5]. Recently, several studies on the homogenisation of dual-component samples (block/pellets; pellets/powder; block/block) have been published [6, 7]. Although these studies reported a high degree of homogenisation, the homogenisation was determined as being incomplete at full saturation. The final density gradient can be partially attributed to the initial conditions, but it may be also influenced by the hydration process [6], [8, 9] or wall friction [7, 10]. This paper is focused on the investigation of the homogenisation properties of BCV bentonite as evaluated under laboratory conditions for two component block/block samples of different initial dry densities.

2 Materials and methods

2.1 BCV bentonite

BCV bentonite is a natural bentonite mined at Černý Vrch deposit in the north-western part of the Czech Republic. It is produced industrially in the form of a powder with water content of 11%. The bentonite is composed of Ca/Mg montmorillonite (69.7%), quartz (11.4%), kaolinite (5.0%), illite (3.7%), Mg-calcite (3.7%), goethite (3.1%) and anatase (2.3%). The cation exchange capacity reaches 60.9 meq/100 g [11], the liquid limit is 135 ± 5% and the plastic limit 48 ± 5% [11, 12]. Further details on the geochemical and geotechnical parameters can be found in [11] and [13].

2.2 Experimental methods

The laboratory experiments were carried out in constant volume "MPC" cells. Bentonite samples were prepared by static uniaxial compaction of the BCV powder into

* Corresponding author: najser@natur.cuni.cz

test cells. The presented tests included experiments performed on two single-density and two dual-density samples.

The single-density samples were prepared in the form of two layers separately compacted to the same target dry density (1.3 and 1.7 g/cm^3 respectively). Each layer consisted of 36 grams of the powder. The stainless-steel constant volume cells for single-density tests are shown in Fig. 1a. Diameter of the samples was 50 mm and the total heights varied in the range 18-26 mm (Table 1) based on the required initial dry density. The samples were saturated with deionised water through the bottom base with only minimal water pressure gradient of 5 kPa. The increase in the swelling pressure was monitored until a constant value was reached.

The dual-density tests were prepared in a similar way to the single-density samples but with differing compaction forces for each sample layer. Both dual-density samples were identical, but different saturation direction was applied during the tests. The dual-density experiments included the monitoring of the swelling pressure at both ends, which resulted in the symmetrical arrangement of the cell (Fig. 1b).

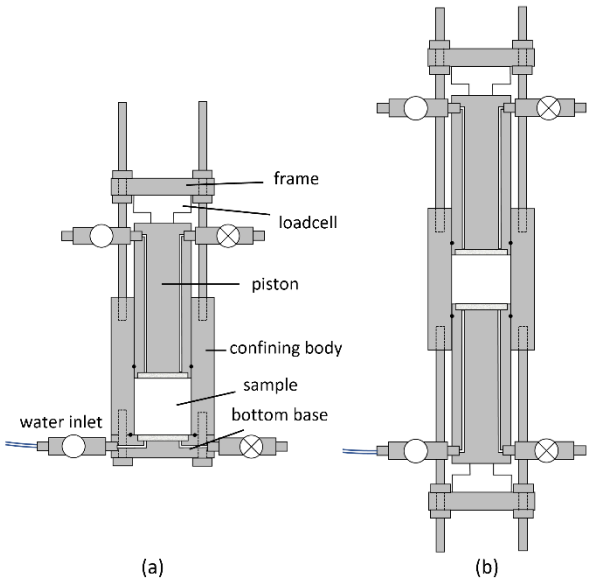

Fig. 1. "MPC" constant volume cells used for (a) single-density and (b) dual-density experiments.

Table 1. Summary of the experiments.

Type of test	Target dry density (g/cm^3)		Total sample height (mm)
	Top layer	Bottom layer	
Single density	1.3	1.3	25.95
Single density	1.7	1.7	21.78
Dual density	1.7	1.3	22.45
Dual density	1.3	1.7	22.36

3 Laboratory test results

The swelling pressures determined from single-density tests are plotted in Fig. 2 in comparison with larger set of results obtained on single-layer BCV samples, reported in [11]. The new results exhibit the same trend of the swelling pressure with the dry density and confirms the consistency of the results.

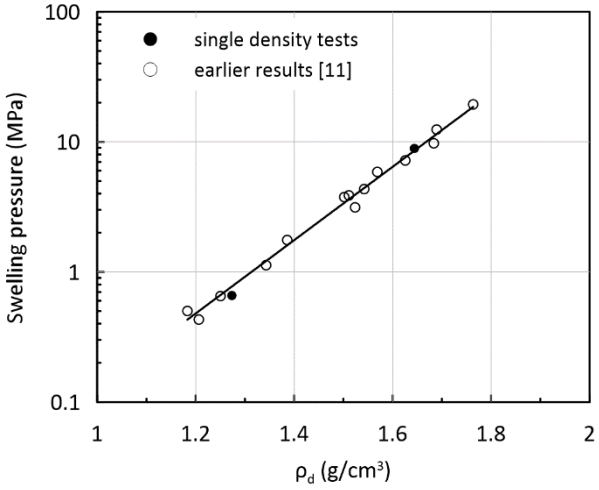

Fig. 2. Dependency of the swelling pressure on the dry density.

In dual-density samples, the time-evolution of the swelling pressure during saturation was found to differ significantly for two different saturation directions (Fig. 3a). Sample saturated from the high dry density end exhibited a rapid increase in the swelling pressure at both ends during the initial saturation phase due to the high swelling potential of the high-density layer. As saturation proceeded to the other layer, the homogenisation of the whole of the sample took place and the swelling pressure at both ends decreased. The development of the swelling pressures in sample saturated from the low-density layer was significantly slower with no peak observed on the swelling pressure curves. It can be explained by the expansion of the high-density layer during the saturation thereof and the resulting compression (densification) of the low-density layer, which had already been saturated and, thus, behaved in a plastic and more deformable manner.

The swelling pressures reached steady values after approximately 400 hours in sample saturated from high-density layer, while the saturation of the other dual density sample was significantly faster. This difference can be explained by different hydraulic conductivities of bottom layers and consequently a different rate of saturation.

Fig. 3b provides a comparison of the swelling pressure evolution in dual-density and single-density samples, which represent the behaviour of the individual layers. It reveals that the swelling pressures of the individual layers (8.9 and 0.7 MPa, respectively) reached 2.6 and 2.1 MPa on the respective bases of the dual-density samples. The measured difference, which was only 0.5 MPa with the higher swelling pressure corresponding to the layer with the higher initial dry density, can be attributed to the side friction. Despite the

significantly differing evolution of the swelling pressures in the two dual-density samples, the final values were almost identical for both tests. This indicates that the direction of saturation has no significant effect on the final swelling pressure.

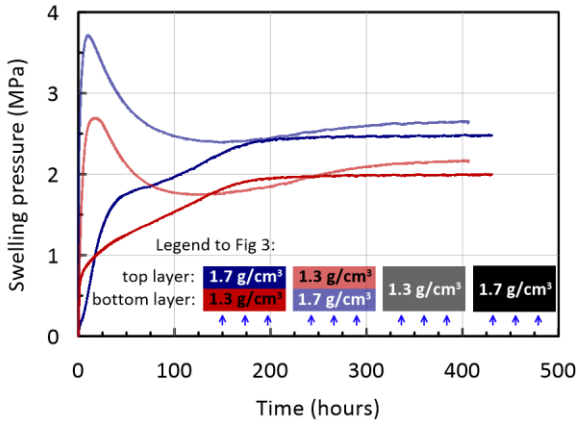

(a)

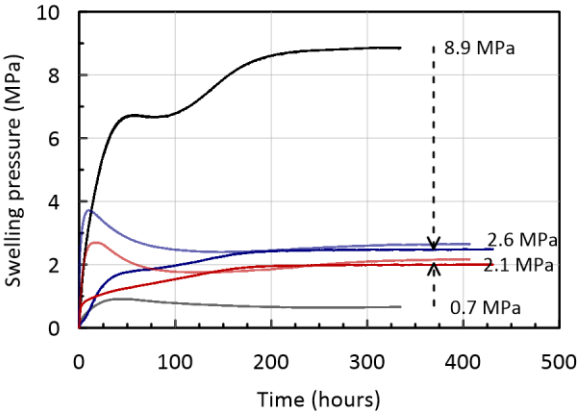

(b)

Fig. 3. Evolution of the swelling pressures in the dual-density samples compared with the single-density tests.

A comparison of the swelling pressures after full saturation is presented in Fig. 4. The average dry densities of the dual-density samples were calculated based on the assumption of constant volume conditions. Both single- and dual-density samples follow the same trend, which is in line with the average trend obtained from a larger set of single-layer BCV samples [11].

The process of homogenisation was studied by the determination of the final density profiles of the dual-density samples. The samples were carefully extracted from the cells and cut into thin slices parallel to the sample bases. The dry density profiles of the samples were calculated from the measured water content with the assumption that the samples had reached full saturation (Fig. 5). The layers close to the saturation base were observed to have been partially affected by the absorption of water from porous stones during the dismantling of the cells, which resulted in swelling (dotted lines in Fig. 5). The straight bold lines represent the initial density profile before saturation.

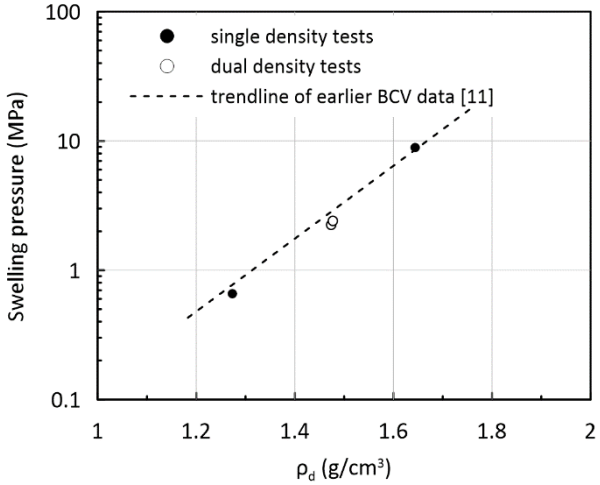

Fig. 4. Comparison of the average final swelling pressures of the single-density and dual-density samples.

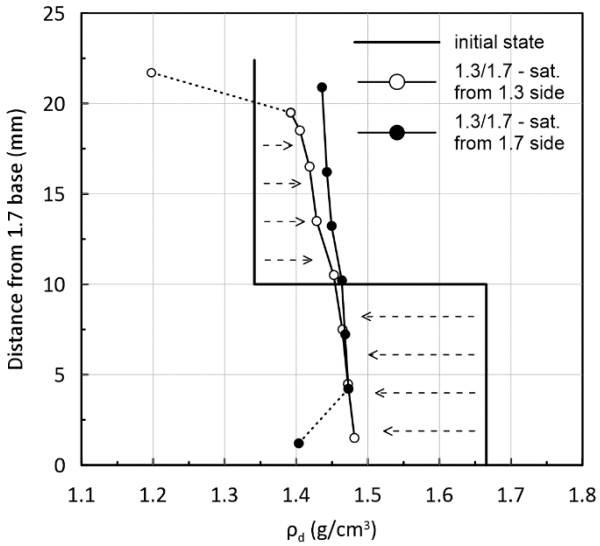

Fig. 5. Vertical distribution of the initial and final dry densities in the dual-density samples.

Both samples provided relatively consistent final dry density profiles. They indicate the homogenisation of the dry density across the samples, with a maximum difference of approximately 0.1 g/cm^3 between the top and bottom parts. Both profiles also show a gradual change in the dry density over the height of the samples with no distinct border between the two layers. Further, very similar dry density profiles were obtained for both samples, which served to indicate that differing saturation directions exert no distinct impact on the final dry density distribution, although temporal evolution of swelling pressure was substantially different in the two cases.

4 Numerical simulations

The laboratory experiments were simulated by means of a thermo-hydro-mechanical hypoplastic model for bentonite [14, 15] implemented in the SIFEL coupled finite element code [16]. The calibration and validation of the model using data obtained from BCV bentonite

laboratory (single-density) samples, details of which are available elsewhere [13], proved its high level of performance with respect to experiments of various types when modelled using a single parameter set. The experiments used for calibration purposes included the testing of swelling pressure and oedometric swelling under constant loading at differing initial dry densities, the oedometric loading and unloading testing of saturated samples, water retention tests under confined and free swelling conditions at various initial dry densities and the uniaxial compression testing of unsaturated samples.

With respect to this study, the most relevant consideration concerns the response under constant volume conditions. Figure 6 shows the reached swelling pressure during constant volume swelling pressure tests for various dry densities. While the model slightly overpredicted the swelling pressures at low dry densities, in general the predictions can be considered to be accurate. A summary of the parameters of the model, as calibrated in [13], is presented in Table 2.

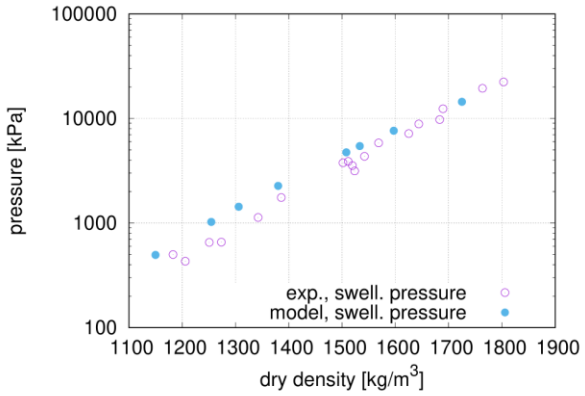

Fig. 6. Dependency of the swelling pressure on the dry density.

Table 2. Parameter values of the THM hypoplastic model for BCV bentonite [13].

Parameter	Unit	Value
φ_c	°	25
λ^*	–	0.12
κ^*	–	0.02
N	–	1.62
υ	–	0.24
n_s	–	0.01
l_s	–	0.0
n_T	–	-0.07
l_T	–	0
m	–	10
α_s	$1/K$	0.00015
κ_m	–	0.1
s_r	kPa	-1000
e_{r0}^m	–	1.0
c_{sh}	–	0.1
s_{e0}	kPa	-2,700
e_0^M	–	0.50
T_r	K	294
a	N/m	0.118
b	$N/(mK)$	-0.000154
a_e	–	0.75
λ_{p0}	–	1.2

The single- and dual-density tests described in this study were simulated using finite elements as boundary value problems, while considering permeability dependent on the porosity and degree of saturation governed by the following relationship:

$$k = k_0 e^{[b(n-n_0)]}(S_r)^{\lambda} \quad (1)$$

where k is the permeability, k_0 is the saturated permeability at a reference porosity of n_0, n is the porosity, S_r is the degree of saturation, b is a parameter that controls the dependency of the permeability on the porosity, and λ is a parameter that controls the dependency of the permeability on S_r. The permeability parameters were set by a trial-and-error procedure through the calculation of the swelling pressure versus time evolution curves, as summarised in Table 3.

Table 3. Values of the permeability control parameters.

Parameter	Unit	Value
k_0	m^2	$2*10^{-20}$
n_0	–	0.46
b	–	20
λ	–	3.0

The simulations of swelling pressure time evolution curves of dual-density samples are shown in Fig. 7. The model represented to a high level of accuracy the final swelling pressures for both the single- and dual-density samples. While the accuracy of the simulations of the single-density samples was unsurprising since equivalent data were used for the calibration of the model, the good prediction of the swelling pressures of the dual-density samples demonstrated the ability of the model to represent more complex homogenisation problems.

The model also predicted relatively well the transient parts of the swelling pressure evolution curves prior to full saturation, including the occurrence of a noticeable swelling pressure peak for the dual-density sample saturated through the high-density layer when compared with the gradual swelling pressure evolution observed for the dual-density sample saturated through the low-density layer.

The most pronounced discrepancy concerned the rapid swelling pressure increase immediately prior to the sample reaching full saturation, which was subsequently followed by a constant pressure. This model response, caused by adopted formulation of water retention curve, should be corrected in the future version of the model.

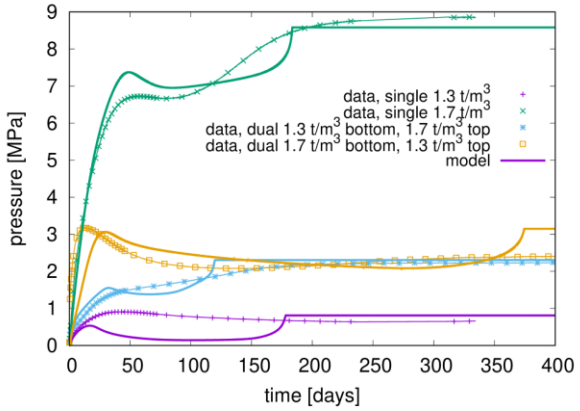

Fig. 7. Swelling pressure time evolution curves as observed experimentally and as predicted by the model with n- and Sr- dependent permeability.

In order to demonstrate the effect of state-dependent permeability, the simulations were repeated with a constant permeability k equal to $5*10^{-20}$ m^2, calibrated in such a way that the state of full saturation was predicted reasonably well for all the simulated samples. The swelling pressure evolution curves are shown in Fig. 8.

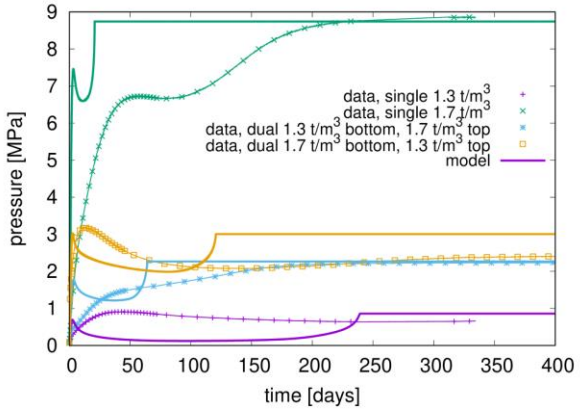

Fig. 8. Swelling pressure time evolution curves as observed experimentally and as predicted by the model with constant permeability.

Constant permeability leads to the over-prediction of the saturation rate in the initial phases of the experiment, at which point the real unsaturated permeability is significantly lower than the assumed constant permeability due to the low value of the degree of saturation. The saturation rate is over-predicted for the high-density sample (the real permeability is lower than the assumed constant permeability due to the lower porosity) and under-predicted for the low-density sample.

Fig. 9 illustrates the distribution of dry density across the sample, as simulated by the n- and S_r- dependent permeability model. Unlike the swelling pressure evolution curves, which were predicted well by the model, the tendency towards "homogenisation" (the equalisation of the dry density across the sample) was not reflected well by the simulations. The model correctly predicted the trend towards a decrease in the dry density for the high dry-density end and an increase in the dry density for the low dry-density end. However, the experiment demonstrated the relatively gradual distribution of dry density with the height of the sample, whereas two distinct dry density sections remained in the modelled case.

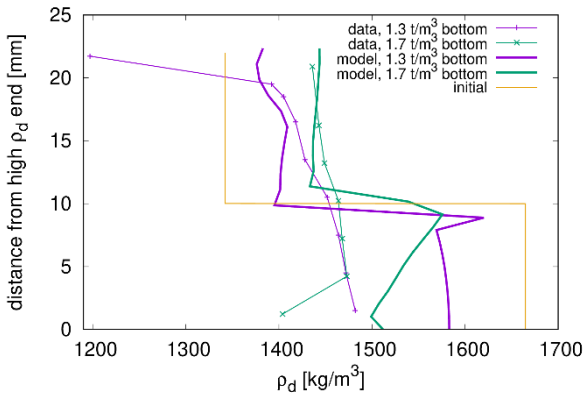

Fig. 9. Distribution of dry density within the samples, comparison of the measured and simulated (state-dependent permeability) curves.

5 Conclusions

The homogenisation behaviour of Czech BCV bentonite was studied by dual-density samples composed of two compacted blocks of differing initial dry densities.

Significantly different swelling pressure evolutions during hydration were recorded for the two identical samples tested, while saturating them from different ends. The samples saturated from the high-density layer exhibited a rapid increase in swelling pressure at both ends, followed by a decrease and a final increase up to a constant value at full saturation. The development of swelling pressures in the samples saturated through the low-density layer was markedly slower and without the appearance of a distinct peak during hydration.

No impact of the saturation direction on the final swelling pressure was identified despite the differing evolution of swelling pressure. The final swelling pressures were consistent with the dry density vs. swelling pressure trend measured on single-density samples, if overall dry density of the dual density sample was considered. The swelling pressures measured at the opposite ends of the samples were slightly different, which can be attributed to the side friction. This difference between the two bases was similar for the both dual-density samples irrespective of the direction of saturation.

The homogenisation was evaluated by the post-mortem determination of the final dry density distribution in the vertical direction. The density profiles confirmed the high degree of homogenisation of the two layers with only small remaining density gradient. The density profiles indicated a gradual change over the height of the samples without the occurrence of a distinct border between the two layers.

Numerical modelling represented to a good degree of accuracy the final swelling pressures and the swelling pressure evolution curves for both the single- and dual-density samples when the porosity and the degree of saturation-dependent permeability was considered. It

was demonstrated that the assumption of constant permeability led to the over prediction of the swelling pressure increase rate in the initial phases of the experiment, the overall over prediction of the saturation rate for the high dry-density samples and the under prediction for the low dry-density samples.

The model, however, failed to fully capture the homogenisation of dry density for the dual-density experiments. While the tendency towards homogenisation was predicted accurately, two distinct density zones remained in the simulations of the dual-density samples.

6 Acknowledgements

The authors would like to thank H. Sun and K. Mach for their assistance in swelling pressure measurements and M. Takáč for the development of experimental equipment. The authors are grateful for the financial support provided by the BEACON (Euratom research and training programme 2014-2018 under grant agreement No. 745942) and EURAD (European Union's Horizon 2020 research and innovation programme under grant agreement No 847593) research projects.

References

1. C. Imbert, M.V. Villar, Appl. Clay Sci. **32** (2006)
2. O. Karnland, U. Nilsson, H. Weber, P. Wersin, Clays in Nat. & Eng. Barriers for Rad. Waste Conf. **33** (2008)
3. R. Pusch, P. Bluemling, L. Johnson, Appl. Clay Sci. **23**(1) (2003)
4. M. Van Geet, G. Volckaert, S. Roels, Appl. Clay Sci. **29** (2005)
5. A. Molinero Guerra, P. Aimedieu, M. Bornert, Y.J. Cui, A.M. Tang, Z. Sun, N. Mokni, P. Delage, F. Bernier, Appl. Clay Sci. **165** (2018)
6. M.V. Villar, R.J. Iglesias, C. Gutiérrez-Álvarez, B. Carbonell, Eng. Geol. **264** (2021)
7. F. Bernachy-Barbe. Homogenization of bentonite upon saturation: Density and pressure fields. Appl. Clay Sci. **209** (2021)
8. F. Bernachy-Barbe, N. Conil, W. Guillot, J. Talandier, Appl. Clay Sci. **189** (2020)
9. Z.R. Liu, Y.J. Cui, W.M. Ye, B. Chen, Q. Wang, Y.G. Chen, Acta Geotech. **15** (2020)
10. Z. Zeng, Y.-J. Cui, N. Conil, J. Talandier, Acta Geotech. **16** (2021)
11. F. Laufek, I. Hanusová, J. Svoboda, R. Vašíček, J. Najser, M. Koubová, M. Čurda, F. Pticen, L. Vaculíková, Minerals, **11**, 871 (2021)
12. R. Červinka, R. Vašíček, P. Večerník, V. Kašpar, Tech. Rep. SÚRAO TZ419/2019 (SÚRAO, Prague 2018)
13. J. Svoboda, D. Mašín, J. Najser, R. Vašíček, I. Hanusová, L. Hausmannová, Acta Geotech. (2022)
14. D. Mašín, Eng. Geol. **165** (2013)
15. D. Mašín, ASCE J. of Eng. Mech. **143**, 9 (2017)
16. T. Koudelka, T. Krejčí, J. Kruis, Proc. of Int. Conf. on Num. Analysis and Appl. Math., **1978** (New York, 2018)